BL33XU
TOYOTA

1. Introduction

The BL33XU Toyota beamline was built in FY2009 and is operated by Toyota Central R&D Labs., Inc. [1]. The original purpose of this beamline was to perform quick-scanning X-ray absorption spectroscopy (QXAFS) for operando analysis and three-dimensional X-ray diffraction (3DXRD). These techniques were unavailable at SPring-8 before 2009 but were needed for industrial applications. In addition to these, the following techniques have been adopted: X-ray diffraction (XRD), X-ray computed tomography (CT)/laminography, and small-angle X-ray scattering (SAXS), as shown in Fig. 1. In this report, we describe the current status of this beamline and recent technical progress.

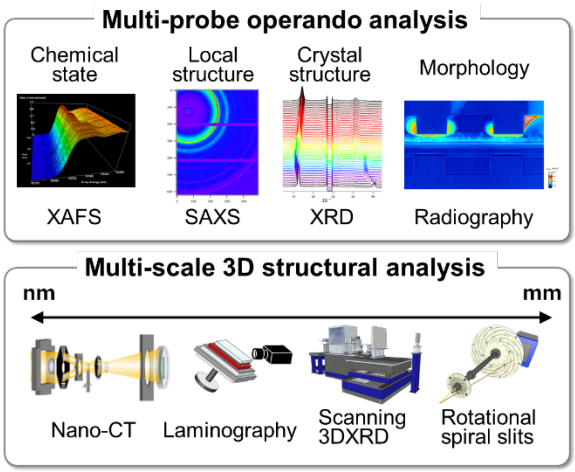

Fig. 1. Measurement techniques at BL33XU.

2. BL33XU beamline

2-1. Beamline layout

The medium-length beamline of BL33XU has the optics hutch in the storage ring building of SPring-8. The experimental facility building is located outside the storage ring building. It has three experimental hutches, a chemical laboratory, and an office room.

The layout of the optical components of BL33XU, where two different types of monochromators are installed, is shown in Fig. 2. Optics 1 is mainly used for QXAFS. It is composed of horizontal deflection mirrors (M1 and M2) in the optics hutch, compact monochromators (C-Mono) with channel-cut crystals, and vertical deflection mirrors (M3 and M4) in EH1. Optics 2 is used for 3DXRD and other techniques. It consists of a SPring-8 standard double-crystal monochromator, vertical deflection mirrors (M4 and M5), and Kirkpatrick–Baez focusing mirrors (KBM) that yield a 1-μm-square microbeam at 50 keV in EH3.

2-2. Analysis techniques

(1) QXAFS

A tapered undulator combined with the servo-motor-driven channel-cut monochromator realizes the rapid data acquisition of XAFS with a temporal resolution of 10 ms [2]. The energy range from 4.0 to 45 keV is accomplished by the two monochromators with Si(111) and Si(220) crystals. This QXAFS system has enabled the development of various *in situ* measurement techniques such as the simultaneous XAFS and XRD measurements of

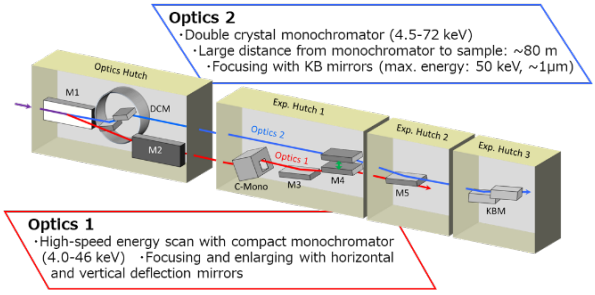

Fig. 2. Optical components of BL33XU.

positive and negative electrodes of lithium-ion batteries during charging and discharging [3].

(2) SAXS

For SAXS at BL33XU, the camera distance can be selected from tens of centimeters to 4.5 meters. A two-dimensional detector, PILATUS 300K (Dectris), is available for the developed *in situ* measurement system. A sample task is an *in situ* measurement to analyze the structural evolution of resins during injection molding [4].

(3) XRD

To analyze the reliability of mechanical and electronic components, it is important to measure the internal stresses and strains nondestructively. The measurement based on XRD was realized by using a multi-axial goniometer equipped with a newly developed rotating and revolving spiral slits system. The rotating shield disks with the slits enable the detection of diffraction only from a small gage volume of interest inside a component with a two-dimensional detector, PILATUS. This system realizes the depth-resolved distribution measurement of strains in an actual mechanical component [5].

(4) Scanning 3DXRD

To measure the three-dimensional distribution of stresses inside the grains of a bulk sample, i.e., type III stresses, the scanning three-dimensional X-ray diffraction (3DXRD) microscopy methodology was developed [6]. This nondestructive technique was validated in 2013, and the three-dimensional distribution of stresses inside the grains of bulk polycrystalline steel under tensile deformation was measured in 2019 [7]. The results revealed that the microscopic intragranular stresses considerably deviate from the macroscopic average stresses measured by conventional methods. Combined with other nondestructive measurement techniques such as XRD and laminography, 3DXRD is expected to facilitate the development of multiscale material modeling that expresses the deformation, fracture, and life of components.

(5) X-ray CT and laminography

To meet the growing need for the high-resolution, nondestructive observation of internal behavior in mechanical and electronic components, X-ray CT and laminography techniques were introduced. The resolutions of the two imaging techniques are higher than 1 μm, even under *in situ* measurement, where sample materials and components are exposed to actual working conditions. A newly adopted CT system with a Fresnel zone plate (FZP) has achieved a resolution of ~100 nm.

3. Recent progress: *Operando* radiography for visualizing liquid water in polymer electrolyte fuel cell

Polymer electrolyte fuel cells (PEFCs) have been utilized as power sources for automotive applications; however, further improvements in power density are still required. A PEFC consists of a catalyst-coated membrane (CCM) sandwiched between gas diffusion layers (GDLs), which are in turn enclosed by bipolar plates with flow fields, as shown in Fig. 3(b). One of the primary causes of performance degradation is oxygen transport resistance through the GDLs. This resistance can become significant owing to the accumulation of liquid water, a by-product of PEFC operation.

To understand water transport phenomena, *operando* synchrotron X-ray radiography was applied at BL33XU [8,9] to visualize the liquid water. In previous studies, small cells with a channel length of 6 mm were used, although the channel length in practical PEFCs exceeds 100 mm. Therefore, a new *operando* cell with a channel

length of 100 mm was developed [10].

Fig. 3(a) shows a schematic image of the X-ray radiography setup using the new cell. By moving the cell perpendicular to the X-rays, radiographic images were obtained at 10 positions along the channel direction. The X-ray exposure time was 1.0 s, and the interval between exposures was 0.5 s. Radiographic images were continuously acquired from the beginning of the operation up to 600 s. At each position, the amount of liquid water was evaluated using the Lambert–Beer law described below.

$$t_{\mathrm{water}} = \frac{1}{\mu} \ln \frac{I_{\mathrm{dry}}}{I}$$

Here, t_{water} represents the equivalent water thickness, i.e., the amount of water integrated along the X-ray transmission path (4.05 mm), μ is the attenuation coefficient for water (0.344 $\mathrm{mm^{-1}}$ at an X-ray energy of 11.4 keV), I_{dry} is the intensity of the transmitted X-rays before operation (i.e., without liquid water), and I is the intensity of the transmitted X-rays during cell operation. Figure 3(b) shows the X-ray transmission image before operation at the cathode outlet, and Fig. 3(c) shows an example of the water distribution. The cell was operated at 313 K with air supplied to the cathode and hydrogen to the anode in a counter-flow configuration [the cathode inlet corresponds to the anode outlet, as shown in Fig. 3(a)].

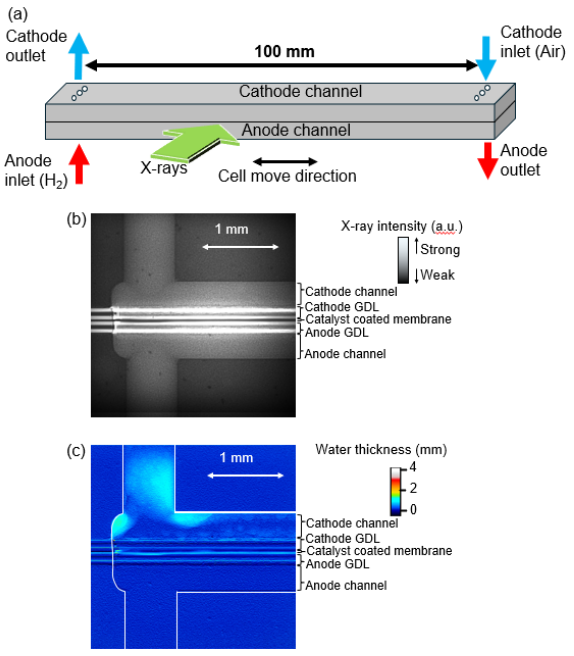

Fig. 3. (a) Schematic image of *operando* radiography of practical sized PEFC. (b) X-ray transmission image at cathode outlet. (c) Example of water distribution at cathode outlet. White line, which indicates the edge of flow field, is added to the figure for visibility.

Figure 4 illustrates the water distribution along the channel direction under steady-state conditions (averaged between 500 and 600 s after the start of operation). In Fig. 4, the water thickness in the cathode GDL increases from the cathode inlet to a distance of 11 mm, then remains nearly constant up to 55 mm, and decreases to zero at the cathode outlet. Moreover, the water thickness in the anode

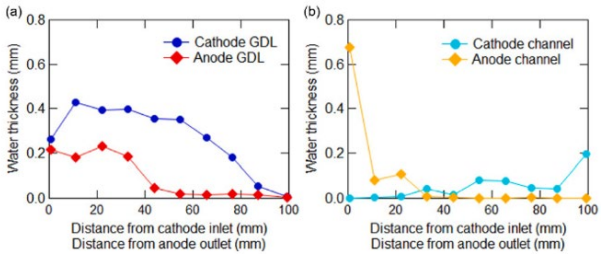

Fig. 4. Relationship between the amount of water under steady state and the distance from the cathode inlet (anode outlet) in (a) GDLs and (b) channels. Reprinted from *Electrochemistry Communications*, **165**, 107772, Akihiko, K. et al., "Operando X-ray radiography of liquid water distribution in 100 mm polymer electrolyte fuel cell channels", Copyright (2024), with permission from Elsevier.

GDL remains nearly constant from the cathode inlet (i.e., anode outlet) to 33 mm, after which it decreases toward the cathode outlet.

This result implies that dry hydrogen supplied from the anode inlet reduces the water thickness in the anode GDL, thereby enhancing water transport from the cathode to the anode side, resulting in decreased water thickness toward the cathode outlet. In contrast, it is considered that gas flow in the channel transports water toward the channel outlet, resulting in a greater accumulation of water at each outlet. As future work, *operando* radiography with different GDLs, channel structures, and operating conditions will be performed to understand water transport mechanisms in detail.

KATO Akihiko
Toyota Central R&D Labs., Inc.

References:

[1] Nonaka, T. et al. (2016). *AIP Conf. Proc.* **1741**, 030043.
[2] Nonaka, T. et al. (2012). *Rev. Sci. Instrum.* **83**, 083112.
[3] Makimura, Y. et al. (2016). *J. Electrochem. Soc.* **163**(7), A1450–A1456.
[4] Harada, M. et al. (2015). *SPring-8 User Experiment Report.* 2015A7003, 2015B7003.
[5] Setoyama, D. et al. (2015). *Proc. MECASENSE. 2015*, 4.
[6] Hayashi, Y. et al. (2017). *SPring-8 User Experiment Report.* 2017A7002, 2017B7002.
[7] Hayashi, Y. et al. (2019). *Science.* **366**, 1492–1496.
[8] Hayashi, D. et al. (2017). *SAE Technical Paper*. 2017-01-1188.
[9] Kato, A. et al. (2022). *J. Power Sources*. **521**, 230951.
[10] Kato, A. et al. (2024). *Electrochem. Commun.* **165**, 107772.